Estimates of the ocular wave aberration from pairs of double-pass retinal images

Ignacio Iglesias, Esther Berrio, and Pablo Artal

Laboratorio de Optica, Departamento de Física, Universidad de Murcia, Campus de Espinardo (Edificio C), 30071 Murcia, Spain

Received December 1, 1997; accepted January 28, 1998; revised manuscript received February 9, 1998

We apply a computational technique to retrieve the wave aberration of the eye from the point-spread function obtained from pairs of double-pass retinal images. The method consists of an adapted pyramidal version of a nonlinear least-squares fitting procedure to a wave aberration expressed as an expansion in Zernike polynomials. Although the procedure provides accurate estimates of the wave aberration, it presents several drawbacks that are discussed in detail. In particular, since a great deal of computational time is necessary to retrieve a single wave aberration, this technique is not useful for real-time applications. We present results of wave aberrations in five normal subjects in the fovea for a 4-mm-pupil diameter. In every case there is a clear presence of comalike aberrations, while the third-order spherical aberration is usually smaller than previous estimates. The root-mean-square error in the retrieved wave aberration, when defocus and astigmatism were corrected, ranges from 0.24 to 0.5 wavelength. The particular values of the aberration coefficients present a large intersubject variability. © 1998 Optical Society of America [S0740-3232(98)00209-9]

OCIS codes: 330.5370, 330.4460, 100.5070.

1. INTRODUCTION

The wave aberration (WA) function completely characterizes the image-forming properties of an optical system.[1] The Seidel aberrations, point-spread functions (PSF's), and optical transfer functions can be computed from the wave-front aberration. In the case of the human eye, the WA's value derives not only from its ability to completely describe the ocular optics but also from the fact that it serves as a very useful tool in ophthalmic design (lenses, contact lenses, or intraocular lenses) and as an index to evaluate the eye's optical quality after refractive surgery. In addition, the application of adaptive-optics techniques in the eye[2–4] for high-resolution retinal imaging or for supernormal vision also requires more precise estimates of the ocular WA.

A large variety of techniques have been proposed to measure the WA in artificial optical systems.[5] Some are based on direct or indirect estimates of the wave front from data of the pupil plane: radial shearing interferometry, point diffraction interferometry, Foucault knife-edge test, or Hartmann–Shack sensor. Other techniques use data on the image plane: the curvature sensor,[6] or computational phase retrieval techniques.[7,8] Only some of these methods have been adapted for use in ophthalmoscopes to measure the WA in the human eye[9]: the Foucault knife-edge test,[10] the objective version of the aberroscope,[11] the Hartmann–Shack sensor,[12,13] or the application of phase retrieval computations to retinal images.[14]

Following this last approach, we have developed an improved and more robust computational procedure to retrieve the wave-front aberration from the ocular PSF obtained from pairs of double-pass retinal images. To correctly estimate all the ocular aberrations, including the asymmetric ones, two different double-pass images have to be recorded. The reason for this requirement is that, since the double-pass image is the autocorrelation of the input and output spread function,[15] when entrance and exit pupil sizes are equal, the information on the odd aberrations and the actual point spread is lost. Using unequal entrance and exit pupil sizes, the double-pass technique permits recording of a low-resolution version of the ocular PSF.[16] From these two retinal images the PSF is reconstructed and serves as input data in the procedure to retrieve the WA. We present here a description of the retrieval method that we developed to determine the WA, together with examples of the WA results obtained in five normal eyes.

2. METHOD

A. Reconstruction of the Point-Spread Function from a Pair of Double-Pass Retinal Images

The complete procedure for obtaining the ocular PSF from a pair of double-pass retinal images was described in detail elsewhere.[17] One of the double-pass images is captured with the same-diameter pupil for the entrance and exit apertures. This corresponds to the autocorrelation of the PSF. The other image is captured with an unequal-pupil-diameter double-pass configuration[16]; one of the apertures, typically the entrance one, is of small diameter (1.5 mm), and the other is of the desired diameter to be measured. This image is a low-resolution version of the ocular PSF or, more precisely, the convolution of the PSF with the spread function corresponding to a 1.5-mm-diameter pupil. We assume that the eye for this small pupil is similar to a diffraction-limited system or, at least, that it produces a radially symmetric retinal image when the small pupil is correctly centered with respect to the natural pupil.[18] We combined these two double-pass im-

ages to reconstruct the actual PSF of the eye by using an iterative phase retrieval algorithm (see Ref. 17 for additional details).

B. Computational Procedure To Retrieve the Wave-Front Aberration from the Point-Spread Function

The ocular PSF, $P(x)$, is related to the wave-front aberration, $W(\nu)$, through the expression

$$P(x) = \left| \mathrm{FT}\left\{ m(\nu)\exp\left[i\,\frac{2\pi}{\lambda}\,W(\nu)\right]\right\}\right|^2, \tag{1}$$

where x and ν are retinal and pupil plane generalized coordinates, respectively; FT denotes Fourier transformation; $m(\nu)$ is the modulus of the pupil function; and λ is the wavelength. Calculation of the WA, $W(\nu)$, from the ocular PSF constitutes a typical phase retrieval problem.[8] Two functions are known: the modulus of the field on the diffraction plane, given by the square root of the PSF, and the modulus of the field on the pupil plane, which corresponds, assuming uniform illumination, to a binary circular mask determined by the aperture radius. This is an approximation because the light distribution in the pupil plane after retinal reflection is no longer uniform owing to the photoreceptor directionality.[19]

The different methods that have been used to solve this inverse problem, the retrieval of the WA from the PSF, can be classified into two main groups: nonlinear parametric optimization methods that provide a modal representation of the WA,[7] and methods based on iterative Fourier-transform algorithms[20] that provide a point-to-point phase map in principal value. In this study we concentrated on the first group of techniques since they are numerically more stable, especially in noisy conditions and with highly aberrated systems, as can be the case in the human eye.

The WA was expressed in terms of a Zernike polynomial expansion[1]:

$$W(\nu,\,\mathbf{a}) = \sum_k a_k Z_k(r,\,\theta), \tag{2}$$

where $\mathbf{a} = \{a_1, a_2, \ldots, a_k\}$ is a coefficients vector and $Z_k(r,\theta)$ represents the polynomial elements of the Zernike basis expressed in normalized polar coordinates (r is equal to unity on the pupil edge). Table 1 shows the first 15 terms of the Zernike polynomial expansion along with the correspondence to Seidel aberrations of each term (Noll's normalization was adopted).[21] We selected the Zernike polynomial expansion because it offers some advantages. For instance, it is an orthogonal basis onto a circular aperture of radius unity; its modes, distributed in pairs with odd and even symmetry, are useful for describing systems not symmetrical with respect to their optical axis, as is the case of the eye; these polynomials present an adequate balance among the coefficients; and, finally, there is a direct relationship between the first terms of the Zernike polynomials and the Seidel aberrations.

The field propagated from the pupil to the diffraction (retinal) plane, according to the Fraunhofer approximation, is[22]

Table 1. Zernike Polynomial Expansion (First 15 Terms) Used in This Study

$\mathbf{a_k}$	$\mathbf{Z_k}(r,\theta)$	Correspondence with Seidel Aberrations
a_1	1	Constant
a_2	$2r\cos\theta$	Tilt
a_3	$2r\sin\theta$	Tilt
a_4	$\sqrt{3}(2r^2-1)$	Defocus
a_5	$\sqrt{6}r^2\sin 2\theta$	Astigmatism
a_6	$\sqrt{6}r^2\cos 2\theta$	Astigmatism
a_7	$\sqrt{8}(3r^3-2r)\sin\theta$	Coma
a_8	$\sqrt{8}(3r^3-2r)\cos\theta$	Coma
a_9	$\sqrt{8}r^3\sin 3\theta$	
a_{10}	$\sqrt{8}r^3\cos 3\theta$	
a_{11}	$\sqrt{5}(6r^4-6r^2+1)$	Third-order spherical
a_{12}	$\sqrt{10}(4r^4-3r^2)\cos 2\theta$	
a_{13}	$\sqrt{10}(4r^4-3r^2)\sin 2\theta$	
a_{14}	$\sqrt{10}r^4\cos 4\theta$	
a_{15}	$\sqrt{10}r^4\sin 4\theta$	

$$G(x,\,\mathbf{a}) = \mathrm{FT}\left\{ m(\nu)\exp\left[i\,\frac{2\pi}{\lambda}\,W(\nu,\,\mathbf{a})\right]\right\}, \tag{3}$$

and the PSF is simply the square modulus of $G(x,\,\mathbf{a})$. We constructed an error function for a given estimation of the parameter vector $\mathbf{a}$ as follows:

$$E(\mathbf{a}) = \sum_x \left[\,|A(x)| - |G(x,\,\mathbf{a})|\,\right]^2, \tag{4}$$

with $|A(x)|$ being the actual modulus of the field on the retinal plane (i.e., the square root of the eye's PSF) and $|G(x,\,\mathbf{a})|$ the modulus retrieved from the WA estimation. This error function has a nonlinear dependence with vector $\mathbf{a}$. The optimization problem consists of searching for the best estimation of the parameter vector $\mathbf{a}$, that is, the value of vector $\mathbf{a}$ that minimizes the error function $E(\mathbf{a})$ and corresponds, therefore, to the maximum-likelihood estimation in the presence of additive noise.[7] The particular nonlinear optimization method employed was the Levenberg–Marquardt (LM) algorithm,[23] a modification of the Gauss–Newton algorithm,[24] which has become a standard in nonlinear optimization problems.

The error function of expression (4) can be approximated by a quadratic form given in a Taylor polynomial expansion by

$$E(\mathbf{b}) \cong E(\mathbf{a}) - \sum_k \beta_k\delta_k + \sum_{kl} \alpha_{kl}\delta_k\delta_l\,, \tag{5}$$

where δ_k is the variation of the a_k parameter, β_k is the gradient vector for the metric, and α_{kl} is its curvature matrix:

$$\beta_k = -\frac{1}{2}\,\frac{\partial E(\mathbf{a})}{\partial a_k}, \qquad \alpha_{kl} = \frac{1}{2}\,\frac{\partial^2 E(\mathbf{a})}{\partial a_k\,\partial a_l}. \tag{6}$$

The variation of each parameter in the direction of minimization of the error is determined by solution of the system of equations

$$\sum_l \alpha_{kl}\delta_l = \beta_k . \tag{7}$$

The strategy of the LM algorithm is to introduce a parameter ϵ in the configuration of the curvature matrix α_{kl}:

$$\begin{aligned} \alpha'_{kl} &= \alpha_{kl}(k \neq l), \\ \alpha'_{kk} &= \alpha_{kk}(1 + \epsilon), \end{aligned} \tag{8}$$

accompanied by a readjustment mechanism that increases or reduces the value of ϵ depending on the evolution of the error $E(\mathbf{a})$. In this sense the algorithm approaches the global minimum by means of the quadratic approximation when it reduces the error or, in the contrary case, primarily by means of the gradient.

Let us now discuss the pyramidal version of the LM algorithm. Although the LM algorithm is a robust optimization procedure, it is not capable of discriminating between global and local minima of the error function. In simulated cases that are similar to the eye in terms of magnitude of aberrations and amount of noise, the algorithm either yields incorrect estimations of the aberrations or requires a very large number of iterations. Therefore, to avoid the stagnation in local minima and to speed the convergence, we applied a recursive pyramidal strategy to the LM algorithm. Here we will refer to this procedure as the LM pyramidal algorithm. In summary, this method consists of applying the LM algorithm to a succession of phase retrieval problems of increasing complexity, corresponding to different subsampled versions of the PSF associated with a particular parameter vector **a**. One generates these subsampled PSF's, related to the same WA map, by increasing the pupil diameter, rescaling the radial coordinate of the Zernike polynomial expansion to equal unity on the pupil edge, and keeping the size of the image the same in both the pupil and the diffraction plane. Figure 1 shows, as an example, three of the sampling cases, with the panels at the bottom corresponding to the actual retrieval problem. By application of this recursive procedure, a series of linked optimization problems associated with the original phase retrieval problem for a fixed number of free parameters is solved in a pyramidal scheme, wherein the topology of the parameter space and the error function changes slightly between consecutive stages. This last condition strongly reduces the probability that a local minimum solution of a particular subsampled PSF problem will be a local minimum solution of the following less subsampled stage. This destabilizes the algorithm and orientates the fitting to a solution closer to the global minimum of the error function. Furthermore, computer simulations have confirmed that the number of local minima in the error function decreases when the sampling rate in the diffraction plane decreases. The pyramidal procedure starts with a pupil radius larger than the actual one (the limit, imposed by the sampling theorem, is $R = W/2$ pixels for a $W \times W$ pixel window) and finishes when the correct pupil size (original PSF sampling rate) is reached, providing the overall process with an initial estimation for a final LM problem, a result much better than the null **a** vector.

C. Computational and Experimental Procedure

The calculations were performed in a Silicon Graphics Power Challenge workstation. The programs were written in *C* under the KHOROS 2.0 software development environment for image processing.[25]

The pyramidal strategy was accomplished by use of an initial normalization radius of 128 pixels (half the window width) and a decrease in the pupil radius R in steps (Δ) of 2 pixels up to a final radius of 86 pixels. A final LM cycle was applied with the actual pupil radius associated with the original sampling rate of the PSF image ($R = 85$ pixels, except for subject PA, for whom $R = 64$ pixels). For each radius, 400 iterations were performed. In all cases the null vector was adopted as the initial estimation of the parameter vector **a**. The LM pyramidal algorithm takes approximately 9 s per iteration when 14 free parameters (corresponding to the first 15 Zernike polynomials) and images of 256×256 pixels are considered. Under these conditions the average total computer time for retrieval of the WA was approximately 20 h. A second pyramidal process with a starting parameter vector that was obtained in the first pyramidal process and with the

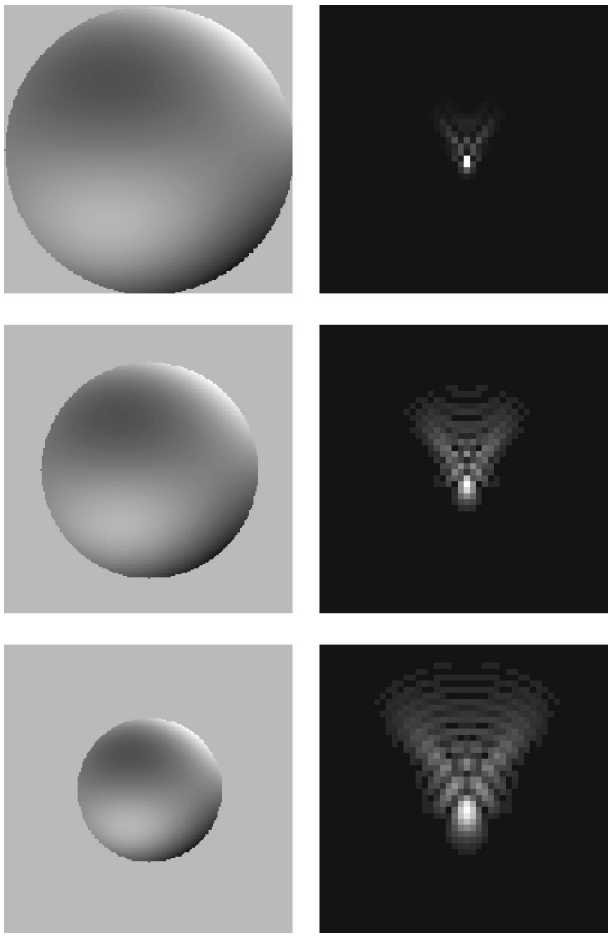

Fig. 1. Schematic diagram of the pyramidal strategy for an optimized phase retrieval (LM pyramidal algorithm). The panels on the right are 64×64 pixel central sections of different subsampled versions of the PSF. The panels on the left are the associated WA maps, for pupil and normalization radius of 128, 96, and 64 pixels, respectively (from top to bottom), within an image size of 256×256 pixels.

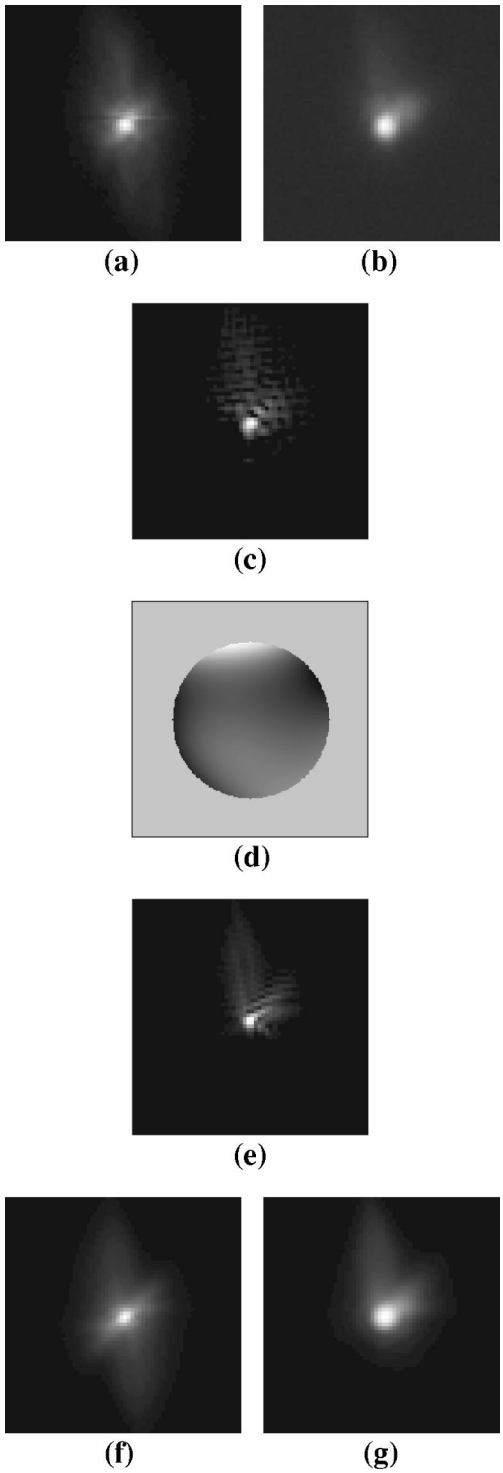

Fig. 2. Sample of results of the whole process of WA retrieval in subject AP. Double-pass images and PSF's subtend 19.8 arcmin. The WA map corresponds to a 4-mm-pupil diameter. (a), (b) Experimental double-pass images recorded with symmetric (4–4 mm) and asymmetric (4–1.5-mm-) diameter pupil size configurations, respectively. (c) Reconstructed PSF from the double-pass images of (a) and (b). (d) Map of the retrieved WA modeled with the first 15 terms of the Zernike polynomial expansion. The gray scale was adjusted between the P–V values. (e) PSF associated with the retrieved WA. (f), (g) Pair of double-pass images computed from the retrieved WA, to be compared with the experimental double-pass images (a) and (b), respectively.

same characteristics as those of the first did not produce a significant reduction in the error. This suggests that the pyramidal scheme induces the algorithm to evolve toward quite stable local minimum positions in the parameter space.

We obtained the WA in five subjects with normal vision. Prior to the collection of the retinal images, every subject passed a complete ophthalmological exam. The retinal double-pass images were collected with paralyzed accommodation [by instillation of two drops of cyclopentholate (1%)], with a 4-mm-diameter artificial pupil, careful centering with respect to the natural pupil, and green light (543 nm). The subjects tested had no clinical values of astigmatism, and their spherical refraction and ages were as follows: AP [−0.75 diopter (D), 24 years old]; PA (−2 D, 35 years old); AG (0 D; 23 years old); NN (+0.25 D, 29 years old); PR (−0.25 D, 29 years old). The pair of double-pass images with equal (4–4-mm) and unequal (4–1.5-mm) pupil size configurations were recorded with the setup and procedure described in Ref. 17. In every subject the images were obtained at the focus position that provided the best image quality.

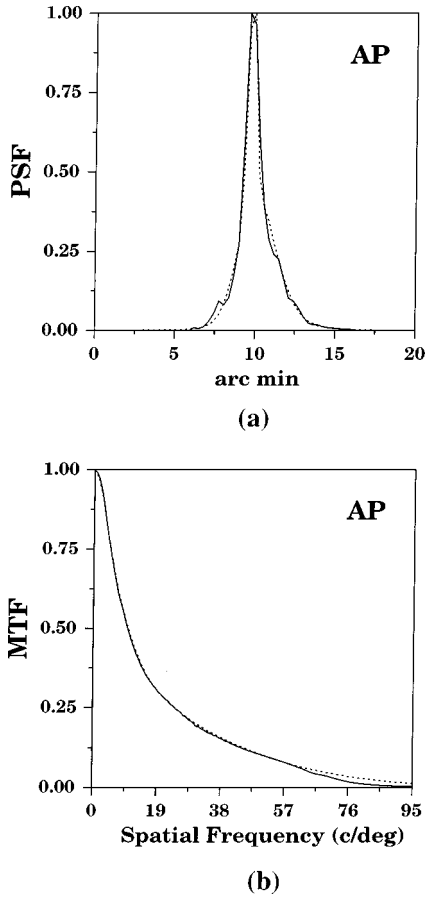

Fig. 3. (a) Comparison between the PSF's (horizontal sections). The solid curve corresponds to the actual data [Fig. 2(c)]; the dashed curve, to the PSF associated with the retrieved WA [Fig. 2(e)]. (b) Comparison of the averaged radial profiles of the modulation transfer functions (MTF's). The solid curve is the MTF computed from the double-pass retinal image [Fig. 2(a)]; the dashed curve, the MTF computed from the retrieved WA.

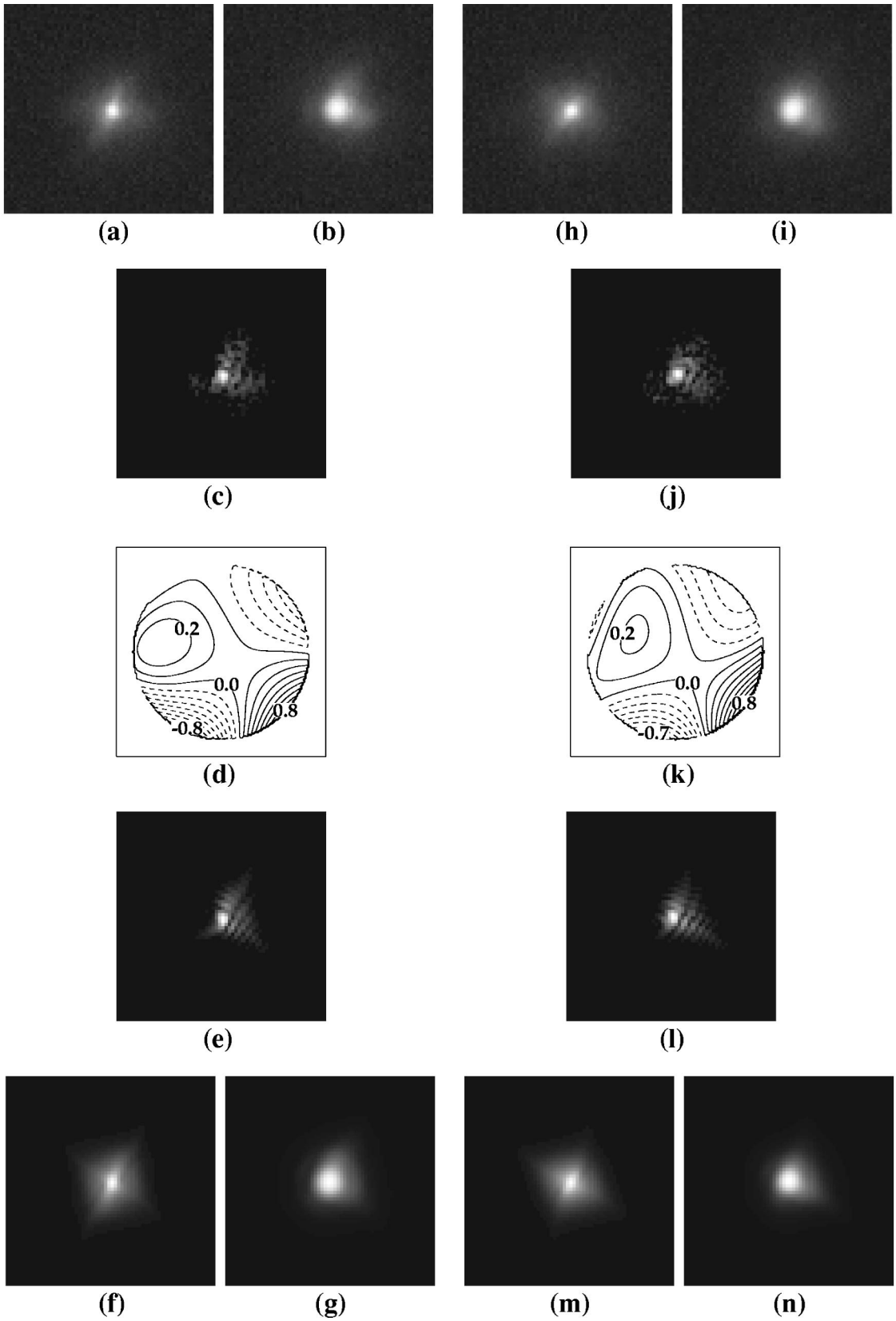

Fig. 4. Two samples of complete results in subject PA corresponding to two different pairs of double-pass images recorded under the same experimental conditions. [(a), (b)], [(h), (i)]: Pairs of experimental double-pass images registered with symmetric pupil configuration of 4–4-mm diameter and asymmetric pupil configuration of 4–1.5-mm diameter. (c), (j): PSF's reconstructed from double-pass images: (d), (k): Maps of retrieved WA's, represented without the coefficients of tilt as contour plots with line steps of 0.1 λ. Dashed curves represent negative values of the aberration. (e), (l): PSF's associated with the WA estimates. [(f), (g)], [(m), (n)]: Double-pass images computed from the retrieved WA's. These images should be compared with the experimental images of panels [(a), (b)], [(h), (i)].

3. RESULTS

Figure 2 presents a sample of the results, showing the complete procedure, in one of the subjects (AP). Figure 2(a) is the autocorrelation of the ocular PSF (obtained with equal 4-mm-pupil diameter in each passage), Fig. 2(b) shows the convolution of the 4-mm ocular PSF and the 1.5-mm near-diffraction-limited pattern, and Fig. 2(c) presents the reconstructed PSF obtained from the pair of double-pass images [Figs. 2(a) and 2(b)]. These three images subtend 19.8 arc min, and the image histogram was slightly modified for improved clarity of the details, especially in the tail of the images. The reconstructed PSF of Fig. 2(c) is used as input data in the retrieval procedure to obtain the WA. Figure 2(d) shows in a gray-level map the obtained WA (the diameter of the circle corresponds to 4 mm in the pupil plane). The peak-to-valley (P–V) range of this WA, expressed in number of 543-nm wavelengths, is 3.65. In the figure, black pixels correspond to approximately -1 wave, and white pixels to approximately 2.6 waves. The other panels in the figure are helpful for evaluation of how accurate the WA estimate is. From the WA, we computed the associated PSF and the corresponding double-pass images. These computed images, showed in Figs. 2(e)–2(g), should be compared with the experimental results of Figs. 2(a)–2(c). In this case, the input images and the images associated with the reconstructed WA are quite similar in both shape and extension. Figure 3(a) shows a comparison of the horizontal sections of the PSF's: the actual data (solid curve), and the PSF associated with the retrieved WA (dashed curve). Figure 3(b) shows a comparison of the averaged radial MTF's: that computed directly from the double-pass image [Fig. 2(a)] recorded with equal pupil diameter (solid curve), and that computed from the retrieved WA (dashed curve). There are some small differences between the PSF's; in particular, the high-spatial-frequency details have not been completely captured. The main reason for this result is that we are modeling the final WA with only 15 terms in the Zernike polynomial expansion. However, with this number of terms (complete third order), we are modeling the most important part of the eye's optics for this pupil diameter.[13] The results shown in Fig. 3 further confirm this, since the MTF's are very similar in the low- and mid-spatial-frequency range, suggesting that the number of terms that we are using is adequate. In addition, the good agreement between the MTF's indicates that the retrieved WA is precise enough to correctly predict the MTF. For high spatial frequencies, the MTF associated with the wave front is higher than that obtained from the double-pass image.

A potential problem of this procedure is how to decide whether the retrieved WA is a correct and realistic estimate or whether it corresponds to a local minimum of the error function, related to a nonrealistic solution. Although one can exactly determine this only when using simulated data, we compared the WA's obtained from the same input PSF, combining a different number of iterations and values of the step parameter Δ in the pyramidal procedure. The Zernike coefficients of the retrieved WA's were relatively similar, showing that, in every case, we were reaching minima that were located in the error space close to one another.

Table 2. Zernike Coefficients (in λ) Obtained from Two Pairs of Double-Pass Images in Subject PA[a]

	Data from PA	
$\mathbf{a_k}$	(2)	(3)
a_1 CTE[b]	0.000000	0.000000
a_2 Tilt x	0.119168	0.120095
a_3 Tilt y	0.039403	0.067154
a_4 Defocus	−0.046165	−0.036906
a_5 Astigmatism y	−0.181802	−0.145588
a_6 Astigmatism x	0.087442	0.095624
a_7 Coma y	−0.006237	−0.013968
a_8 Coma x	0.048557	0.066044
a_9	−0.078176	−0.108839
a_{10}	−0.084068	−0.022084
a_{11} Third-order spherical	−0.003645	0.002921
a_{12}	−0.017268	0.002602
a_{13}	−0.007635	0.006830
a_{14}	−0.001140	−0.030166
a_{15}	0.014478	0.017230

[a] Columns (2) and (3) correspond to the results given in Figs. 4(a)–4(g) and 4(h)–4(n) respectively.
[b] CTE, constant term.

To further test how robust this method for estimation of the WA is, we repeated twice the complete procedure in subject PA for two pairs of double-pass images collected under identical experimental conditions. Figure 4 shows the complete sample of the results for the two cases [Figs. 4(a)–4(g)] and 4(h)–4(n) with the same structure as in Fig. 2: the double-pass images [Figs. 4(a), 4(h) and 4(b), 4(i)]; the reconstructed PSF [Figs. 4(c) and 4(j)]; and the WA's [Figs. 4(d) and 4(k)]. The WA maps are represented as contour line plots with solid and dashed curves for positive and negative values, respectively. The two reconstructed PSF's are similar in shape, although they are slightly rotated with respect to each other, probably because of a different centering during the recording of the double-pass images. The overall shape and absolute value of the aberrations are similar, with a P–V value of 1.73 and 1.66 wavelengths for each case. In addition, in both cases the retrieved WA's clearly follow the main direction of the coma of each input PSF. Table 2 shows the values of the 15 Zernike coefficients in waves for the two retrieved WA's of Fig. 4. Panels (e)–(g) and (l)–(n) of Fig. 4 present the PSF and the double-pass images computed from the WA's, to be compared with the actual data of panels (a)–(c) and (h)–(j) of Fig. 4, respectively.

Figure 5 shows the WA's obtained in the five subjects participating in this study. For each subject (identified by the initials in the left-hand part of the figure), the actual PSF's (left-hand panel), the retrieved WA (central panel), and the associated PSF (right-hand panel) are shown. The PSF's are presented as gray-scale images and subtend 19.8 arc min (except for subject PA, whose PSF subtends 14.7 arc min). The WA's are for a 4-mm-pupil diameter and are represented as contour lines with 0.1 wavelength separation between adjacent lines. The numbers superimposed on the WA graphs represent the values in wavelengths for the particular line. Table 3

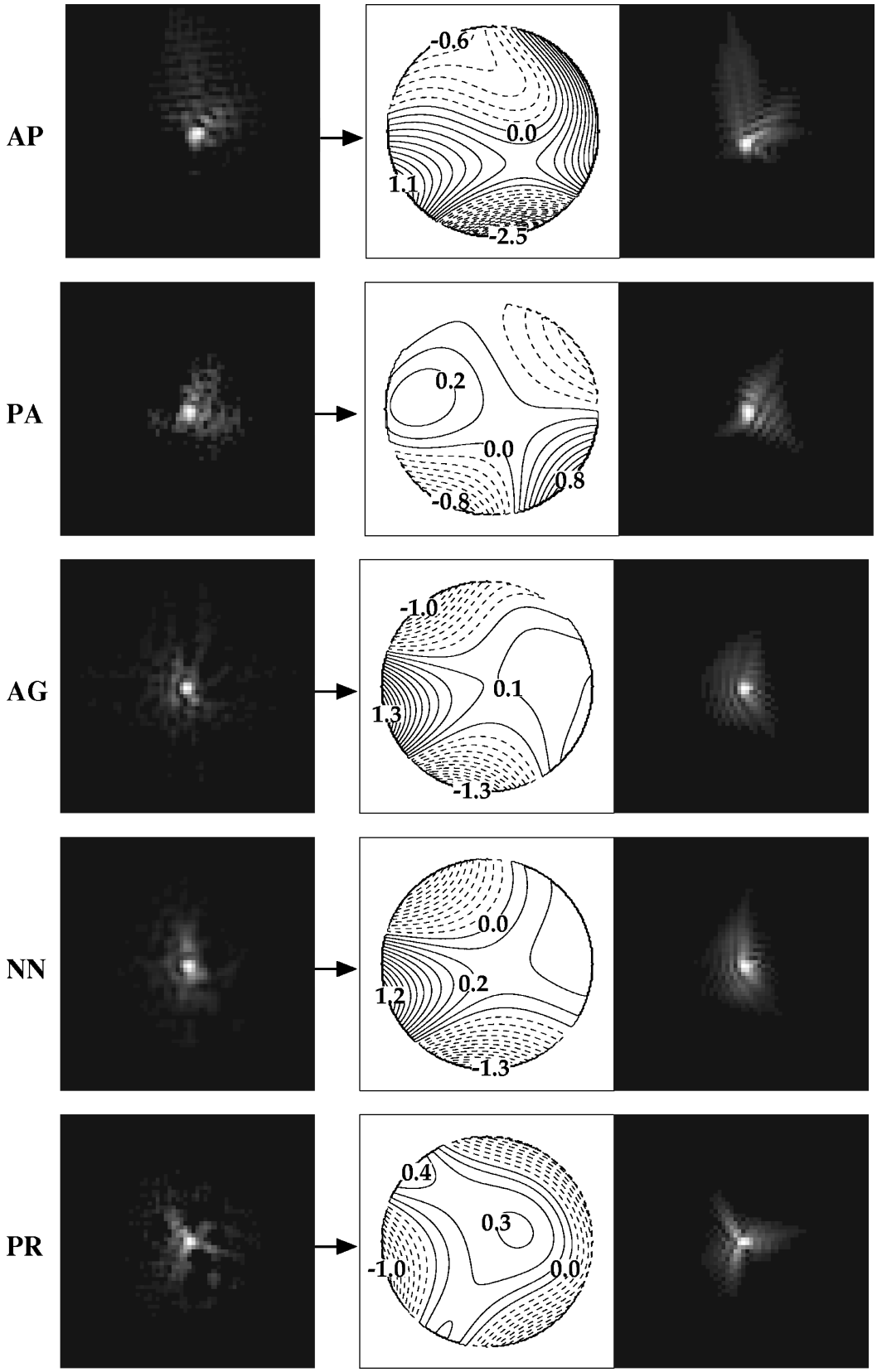

Fig. 5. WA results in the five subjects considered. For each subject (identified by initials on the left), the input PSF (left-hand panel), the retrieved WA (central panel), and the associated PSF (right-hand panel) are represented. The WA's are in contour line graphs (without coefficients of tilt), with 0.1-λ separation among adjacent lines and negative values represented in dashed curves.

Table 3. Zernike Coefficients (in λ) for the Five Subjects Participating in This Study[a]

a_k	Subjects				
	AP	PA	AG	NN	PR
a_1 CTE	0.000000	0.000000	0.000000	0.000000	0.000000
a_2 Tilt x	0.184799	0.119168	−0.147765	−0.111866	−0.018726
a_3 Tilt y	0.356953	0.039403	0.024901	−0.059382	0.038468
a_4 Defocus	0.038801	−0.046165	0.072728	−0.100268	−0.2001
a_5 Astigmatism y	−0.211828	−0.181802	−0.080422	0.186981	−0.037951
a_6 Astigmatism x	−0.349898	0.087442	−0.263914	0.293286	−0.032981
a_7 Coma y	0.178249	−0.006237	−0.004541	0.038017	−0.007575
a_8 Coma x	0.065504	0.048557	0.008972	0.008533	−0.052184
a_9	−0.188917	−0.078176	−0.139822	−0.160408	0.068636
a_{10}	0.055095	−0.084068	−0.163935	−0.125630	0.144763
a_{11} Third-order spherical	−0.009450	−0.003645	−0.012590	−0.005709	−0.035096
a_{12}	0.041647	−0.017268	0.015568	−0.001830	0.002124
a_{13}	0.048223	−0.007635	−0.010445	−0.007950	−0.010593
a_{14}	−0.078782	−0.001140	0.034643	0.017266	−0.044503
a_{15}	−0.036367	0.014478	0.062210	0.033638	−0.061089

[a] The WA maps are in Fig. 5.

shows the values (in wavelengths) of the 15 Zernike coefficients of the WA's in the five subjects. The values of the coefficients a_7 to a_{15} for every subject are also plotted in Fig. 6. From the Zernike coefficients is easy to calculate the values of the Seidel aberrations. In particular, the relationship between coma (A_c) and spherical (A_s) Seidel aberration and the Zernike terms of Table 1 is given by

$$A_c = 3\sqrt{8}\sqrt{(a_7^2 + a_8^2)},$$
$$A_s = 6\sqrt{5}a_{11}. \quad (9)$$

Table 4 presents the values (in wavelengths) of coma and spherical Seidel aberrations for the five subjects. We also calculated several parameters from every WA map: the P–V, the root-mean-square (rms) error, and the associated Strehl ratio, which are shown in Table 5 for the five subjects.

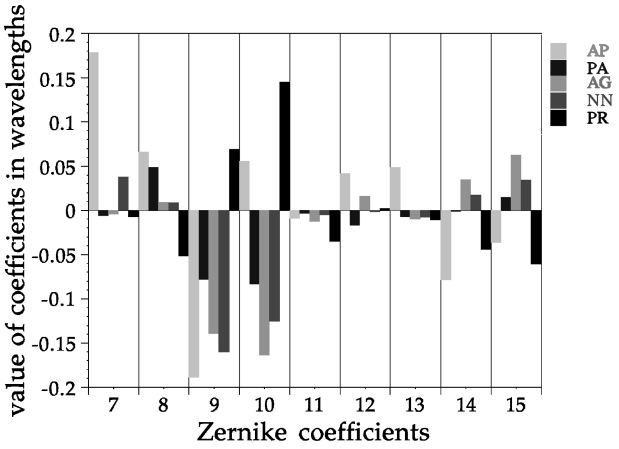

Fig. 6. Values of the Zernike coefficient (a_7–a_{15}) for the five subjects in number of λ.

Table 4. Values (in λ) of the Seidel Spherical and Coma Aberration for the Five Subjects, Computed from Eqs. (9) with the Zernike Coefficients of Table 3

Parameter (in λ)	Subjects				
	AP	PA	AG	NN	PR
Spherical aberration	−0.126	−0.048	−0.208	−0.076	−0.47
Coma	1.272	0.328	0.067	0.261	0.447

4. DISCUSSION

We have developed a procedure to estimate the WA in the human eye from a pair of double-pass retinal images. The results that we obtained in five normal subjects show that the technique produces reliable estimates of the ocular WA. However, the procedure is relatively complicated, and, more importantly, it requires a great deal of computer time for calculation of a single WA. In this section we discuss in some detail the major limitations of the technique, and we compare the results of WA's with previous estimates obtained by other methods.

A. Limitations of the Computational Phase Retrieval Procedure

Two WA's expressed by Zernike polynomials expansions with a simultaneous change of sign in every term of even power of the radial coordinate (r) produce exactly the same PSF. That is, the PSF is invariant to the combined effect of a 180° rotation and an inversion of the WA. This implies that our phase retrieval procedure cannot distinguish between two WA solutions, one corresponding to a given set of values of Zernike coefficients, a_4–a_6 and a_{11}–a_{15}, or a change of sign in all those terms. As a consequence, we always have two possible solutions of the WA, each equally compatible with the PSF data. To select one of the two equally possible solutions, we imposed the condition that the a_{11} coefficient, corresponding to third-order spherical aberration, be negative if it is significatively different from zero. Although this is a some-

how arbitrary selection, it is consistent with most of the previous spherical aberration results for the unaccommodated eye.[26]

A different kind of problem consists in how the noise present in the double-pass images can affect the convergence of the algorithm and the accuracy of the results. Noisy PSF's could induce the retrieval algorithm to stagnate in local minima of the error space, and, as a consequence, the WA estimates would not accurately represent the actual aberrations of the eye. In addition, the retrieval technique performs worst with severely aberrated systems. An intuitive interpretation is that, in these cases, the nonlinear optimization should evolve from a perfect system (with a null parameter vector **a** being used as the starting point) to a final solution with a distant location in the error space. Then the algorithm can easily be trapped in any of the local minima. This limits the application of the procedure to midsize pupil diameters (we present here results for a 4-mm-pupil diameter) and double-pass images obtained at best focus and with the astigmatism corrected.

Table 5. Values of Strehl Ratio, P–V Values, and Root-Mean-Square Error in the WA for Every Subject[a]

Parameter	Subjects				
	AP	PA	AG	NN	PR
Strehl ratio	0.14	0.3	0.2	0.12	0.16
P–V values of the WA (λ)	3.65	1.67	2.74	2.71	1.49
Rms error of the WA (λ)	0.504	0.242	0.364	0.418	0.279

[a] P–V values and rms error are expressed in number of λ.

The WA's modeled with 15 terms in the Zernike expansion could underestimate the aberrations of the eye. Figure 7 shows a comparison of two MTF's in four subjects [the same results for subject AP are shown in Fig. 3(b)]. The MTF's were computed from the double-pass images (solid curve) and from the retrieved WA (dashed curve). Except for subject AG, both curves agree quite well, although the MTF estimated directly from the WA is usually higher than the actual MTF. This suggests that the procedure slightly underestimates the aberrations, inasmuch as we cannot correctly model high-order aberration details in the wave front with only 15 terms in the Zernike expansion. By using a larger number of terms, we would capture more details in the WA, but this would be at the cost of increasing the complexity of the retrieval problem and then decreasing its performance. Modeling the WA with 15 terms is a good choice for the algorithm performance; it completely covers third-order aberrations and is in agreement with recent findings[13] that show that for small- and medium-size pupil diameters the complete third order accounts for most of the ocular aberrations.

Another limitation of the method is that it requires spending a great deal of computer time (roughly 20 h in the computer workstation that we used) to obtain a WA estimation from the PSF. Although it would be possible to decrease by some factor the computer time by optimizing the code, the method is not of use for real-time applications, such as adaptive optics. However, there are a large variety of possible applications in which immediate

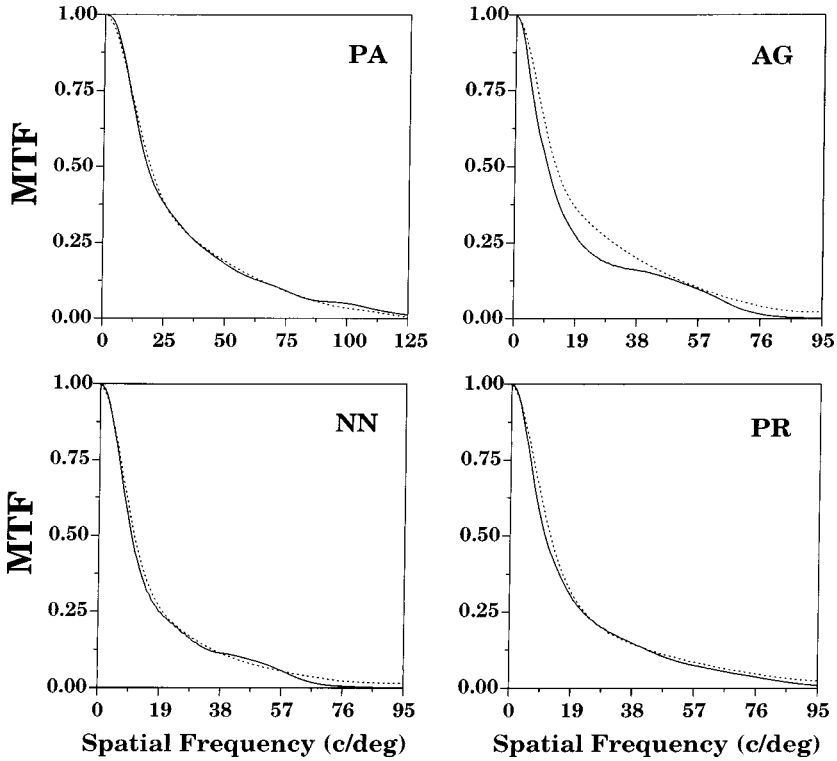

Fig. 7. Comparison of the radial profiles of the MTF's in four subjects (identified by initials). The solid curve is the MTF computed from the double-pass retinal image; the dashed curve, the MTF computed from the retrieved WA.

results are not mandatory and in which this procedure could be successfully applied.

We used estimates of the WA obtained by this procedure to correct the ocular aberrations in the eye, using a liquid-crystal spatial light modulator device.[4] In an artificial eye, the double-pass images after correction of the aberrations were similar to those predicted by computer simulations.[4] This indicates that the retrieval procedure produces accurate estimates of the aberrations and can be considered as additional validation of this retrieval technique.

B. Comparison of the Estimated Wave Aberration with Previous Results

Even when defocus and astigmatism is carefully corrected, the remaining aberrations for a 4-mm-pupil diameter make the eye much worse than a diffraction-limited system. The average rms error for the five subjects is 0.36 λ, five times larger than the common tolerance for diffraction-limited performance (0.07 λ). By contrast, the variability among subjects in the overall ocular aberrations makes the rms error range from 0.24 to 0.5 λ. This result is in agreement with previous measurements of the eye's optical performance that shows quite a large intersubject variability.[11,13,27] One implication of this result is that the use of very general eye models should be considered with caution. In addition, it appears that one needs to use adapted corrections, when considering correction of the ocular aberration.

The results of the Seidel coma aberration were quite significant in several subjects. This further confirms the relative importance of coma in the image quality of the eye in the fovea. In any case, the magnitude of coma shows a clear dependence on the subject: While NN has practically no coma, AP presents more than one wave.

We also analyzed the results of Seidel third-order spherical aberration. Except for one subject, the spherical aberration was lower than 0.1 waves. This is ten times lower than most of the previous estimates,[26,28] where, for a 4-mm-diameter pupil, approximately one wave of spherical aberration was reported. Although intersubject variability could again be a factor to be considered (in fact, one of our subjects has nearly a half-wave of spherical aberration), the most probable reason is that in most of the previous estimates a kind of global radial symmetric aberration was actually measured instead of the pure spherical aberration.

ACKNOWLEDGMENTS

This research was partially supported by Pharmacia & Upjohn (Holland), Dirección General de Investigación Científica y Técnica (Spain) (grant PB94-1138-C02-01), and Region de Murcia (grant COM 6/96). The authors thank Antonio Guirao and Concepción González for help with the double-pass data collection and Pedro Prieto for suggestions on the manuscript.

Address all correspondence to Pablo Artal at the address on the title page or, by e-mail, at pablo@fcu.um.es.

REFERENCES

1. M. Born and E. Wolf, *Principles of Optics* (Pergamon, New York, 1985).
2. J. Liang, D. R. Williams, and D. T. Miller, "Supernormal vision and high-resolution retinal imaging through adaptive optics," J. Opt. Soc. Am. A **14**, 2884–2892 (1997).
3. F. Vargas, I. Iglesias, and P. Artal, "Images of the human fovea after correction of the ocular aberrations with a liquid crystal spatial light modulator," Invest. Ophthalmol. Visual Sci. Suppl. **13**, 513 (1997).
4. F. Vargas-Martin, P. Prieto, and P. Artal, "Correction of the aberrations in the human eye with a liquid-crystal spatial light modulator: limits to performance," J. Opt. Soc. Am. A **15**, 2552–2562 (1998).
5. D. Malacara, *Optical Shop Testing*, 2nd ed. (Wiley, New York, 1992).
6. F. Rodier, "Curvature sensing and compensation: a new concept in adaptive optics," Appl. Opt. **27**, 1223–1225 (1988).
7. W. H. Southwell, "Wave-front analyzer using a maximum likelihood algorithm," J. Opt. Soc. Am. **67**, 396–399 (1977).
8. J. C. Dainty and J. R. Fienup, "Phase retrieval and image reconstruction for astronomy," in *Image Recovery: Theory and Applications*, H. Stark, ed. (Academic, Orlando, Fla., 1987), pp. 231–273.
9. W. N. Charman, "Wavefront aberration of the eye: a review," Optom. Vision Sci. **68**, 574–583 (1991).
10. F. Berny and S. Slansky, "Wavefront determination resulting from Foucault test as applied to the human eye and visual instruments," in *Optical Instruments and Techniques*, J. H. Dickenson, ed. (Oriel, Newcastle, UK, 1969), pp. 375–386.
11. G. Walsh, W. N. Charman, and H. C. Howland, "Objective technique for the determination of monochromatic aberrations of the human eye," J. Opt. Soc. Am. A **1**, 987–992 (1984).
12. J. Liang, B. Grimm, S. Goelz, and J. F. Bille, "Objective measurement of wave aberrations of the human eye with use of a Hartmann–Shack wave-front sensor," J. Opt. Soc. Am. A **11**, 1949–1957 (1994).
13. J. Liang and D. R. Williams, "Aberrations and retinal image quality of the normal human eye," J. Opt. Soc. Am. A **14**, 2873–2883 (1997).
14. P. Artal, J. Santamaría, and J. Bescós, "Retrieval of wave aberration of human eyes from actual point-spread-function data," J. Opt. Soc. Am. A **5**, 1201–1206 (1988).
15. P. Artal, S. Marcos, R. Navarro, and D. R. Williams, "Odd aberrations and double-pass measurements of retinal image quality," J. Opt. Soc. Am. A **12**, 195–201 (1995).
16. P. Artal, I. Iglesias, N. López-Gil, and D. G. Green, "Double-pass measurements of the retinal-image quality with unequal entrance and exit pupil sizes and the reversibility of the eye's optical system," J. Opt. Soc. Am. A **12**, 2358–2366 (1995).
17. I. Iglesias, N. López-Gil, and P. Artal, "Reconstruction of the point-spread function of the human eye from two double-pass retinal images by phase retrieval algorithms," J. Opt. Soc. Am. A **15**, 326–339 (1998).
18. P. Artal, S. Marcos, I. Iglesias, and D. G. Green, "Optical modulation transfer and contrast sensitivity with decentered small pupils in the human eye," Vision Res. **36**, 3575–3586 (1996).
19. S. A. Burns, S. Wu, J. C. He, and A. E. Elsner, "Variations in photoreceptor directionality across the central retina," J. Opt. Soc. Am. A **14**, 2033–2040 (1997).
20. R. W. Gerchberg and W. O. Saxton, "A practical algorithm for the determination of phase from image and diffraction plane pictures," Optik **35**, 237–246 (1972).
21. R. J. Noll, "Zernike polynomials and atmospheric turbulence," J. Opt. Soc. Am. **66**, 207–211 (1976).
22. J. W. Goodman, *Introduction to Fourier Optics*, 2nd ed. (McGraw-Hill, New York, 1996).
23. D. Marquardt, "An algorithm for least-squares estimation of nonlinear parameters," IMA J. Appl. Math. **11**, 431–441 (1963).

24. W. H. Press, B. P. Flannery, S. A. Teukolsky, and W. T. Vetterling, *Numerical Recipes in C* (Cambridge U. Press, New York, 1992).
25. K. Konstantinides and J. R. Rasure, "The KHOROS software development environment for image and signal processing," IEEE Trans. Image Process. **3**, 243–252 (1994).
26. A. Ivanoff, "Les aberrations de chromatisme et de sphericite de l'oeil. Leur role en vison nocturne," Rev. Opt. Theor. Instrum. **26**, 145–171 (1947).
27. H. C. Howland and B. Howland, "A subjective method for the measurement of monochromatic aberrations of the eye," J. Opt. Soc. Am. **67**, 1508–1518 (1977).
28. M. Koomen, R. Tousey, and R. Scoluik, "The spherical aberration of the eye," J. Opt. Soc. Am. **54**, 715–716 (1949).